Available online at www.sciencedirect.com
SCIENCE DIRECT
Journal of Non-Crystalline Solids 352 (2006) 1444–1447
JOURNAL OF NON-CRYSTALLINE SOLIDS
www.elsevier.com/locate/jnoncrysol

UV and ozone influence on the conductivity of ZnO thin films

G. Gonçalves [a,*], A. Pimentel [a], E. Fortunato [a], R. Martins [a], E.L. Queiroz [b], R.F. Bianchi [b,c], R.M. Faria [b]

[a] FCT-UNL/CENIMAT and CEMOP, Campus da Caparica, 2829-516 Caparica, Portugal
[b] Instituto de Física de São Carlos/USP, C.P. 369, 13560-970, São Carlos, Brazil
[c] Escola Politécnica/USP, C.P. 61548, 05424-970, São Paulo, Brazil

Abstract

Complex impedance measurements were used to analyze the influence of ultraviolet and ozone gas on the electronic behaviour of ZnO films grown by rf magnetron sputtering. The data show that UV exposure strongly increases the ac conductivity of the film at very low frequencies, and that after ozone exposure it recovers the original value. At high frequencies, however, UV-light exposure it does not change the conductivity but the ozone acts in the sense to decrease it. Two distinct mechanisms, related to two relaxation time distributions are clearly observed: they are superimposed in the virgin sample, but they split forming two semicircles in the $z''(f) - z'(f)$ diagrams when the samples are treated with UV and/or ozone gas. A combination of the bruggeman effective medium approximation (BEMA) with the random free energy barrier model is used to fit the data and to explain the ac conductivity variation phenomena observed.

PACS: 78.20.e; 73.50.h; 73.20.r; 72.20−i

Keywords: Solar cells; II–VI Semiconductors; Sensors; Conductivity

1. Introduction

Since 1960 zinc oxide has been explored as a versatile material from the point of its electrical properties [1]. More recently, the growing interest in applications of zinc oxide films in varistors, in piezoelectric devices and in acoustic-optical systems has stimulated studies that correlate the film morphology with its electrical properties [2–5]. It is well known that electrical properties of doped-ZnO varistors depend on grain boundary effects, which are, in principle, characteristics of ZnO bulk structure; the granular morphology is responsible for its low conductivity at low fields, but above a critical field, tunneling effect across the potential barriers at the grain boundaries enhances considerably the material conductivity [6]. New deposition techniques, combined with doping, produced conductive and transparent ZnO thin films, providing the exploration of new technological applications as gas sensors [7], transparent electrodes for OLEDs [8], transparent transistors [9], etc. In addition, its (nano-to-micro)granular and (meso)uniform morphologies, whose grain dimensions varies from tenths nanometers to micrometers, permits to obtain a great variety of ZnO nanostructures [10].

The goal of this paper is to progress in the elucidation of the effect of strong conductivity variation of ZnO thin films, deposited by rf magnetron sputtering, when exposed to UV-radiation or to ozone atmosphere [11]. For this, ac measurements were carried out, and a model that takes into account the film morphology was developed.

2. Experimental

ZnO films were deposited by rf magnetron sputtering (S_{rf}-ZnO) onto soda-lime glass substrates at room temperature under pressure of 1.06 Pa. Thicknesses of the films

* Corresponding author. Tel.: +351 212948562; fax: +351 212948558.
E-mail address: gpg@fct.unl.pt (G. Gonçalves).

0022-3093/$ - see front matter © 2006 Elsevier B.V. All rights reserved.
doi:10.1016/j.jnoncrysol.2006.02.021

were measured by the stylus method, being around 200 nm. Aluminum electrodes were vacuum evaporated forming a coplanar gap of 1.6 mm, each leg being 10 mm long. Alternating impedance measurements were performed by a frequency response analyzer (Solartron, 1260 Impedance/Gain phase Analyzer) in the 1–10^6 Hz frequency range. A real impedance plateau usually observed at low frequencies is named dc effective impedance. Most of the experiments were performed at room temperature, but to check the effect of temperature on the electrical response of the samples, some measurements at low temperatures were also performed. Samples were also illuminated by 0.5 mW/cm^2 of 380 nm UV-light during 20 min and exposed to weak ozone atmosphere pressure for 8 h.

3. Results and discussion

Real and imaginary components of impedance measurements carried out with a S_{rf}-ZnO sample, as deposited (virgin sample), were shown in Fig. 1(a). We observed that for low frequencies the real component $z'(f)$ exhibits a plateau (hereafter called dc effective conductivity value, as mentioned in Section 2) at about 90 MΩ that extends up close to 100 Hz; beyond this frequency, denominated here as the critical frequency f_c, the impedance decreased continuously, and at 1 MHz the recorded value of z' was 500 Ω. The imaginary part, $z''(f)$, showed a broad peak with the maximum around f_c. After exposing the sample for 20 min under UV-light, the measurement was repeated at the same conditions (Fig. 1(b)). We observed that, while the dc

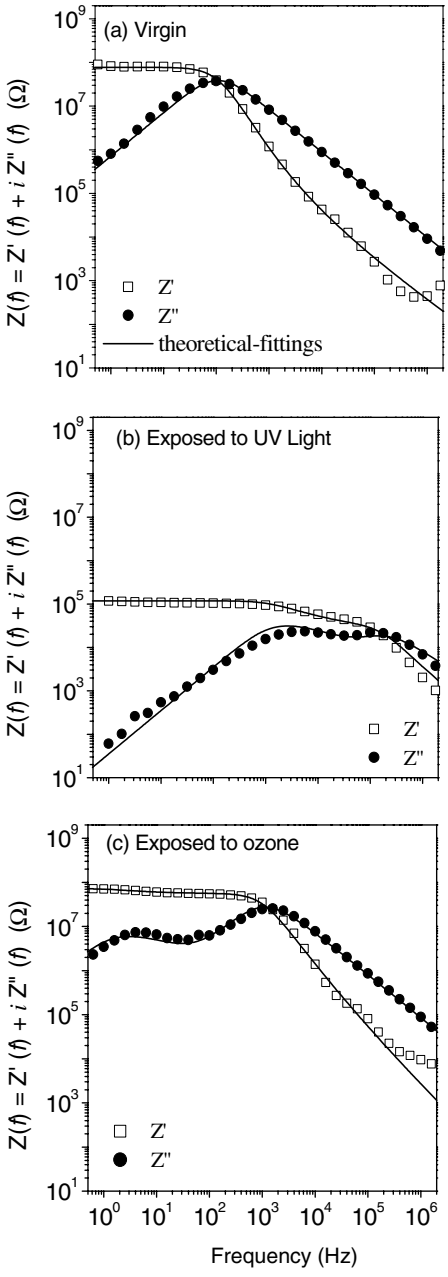

Fig. 1. Real, $z'(f)$, and imaginary, $z''(f)$, components of the complex impedance obtained from: (a) rf sputtering deposited ZnO film, (b) the same film after being irradiated by UV-light for 20 min; and (c) in the sequence, sample exposed to ozone atmosphere for 8 h. Full lines represent the experimental-fittings obtained from Eq. (3).

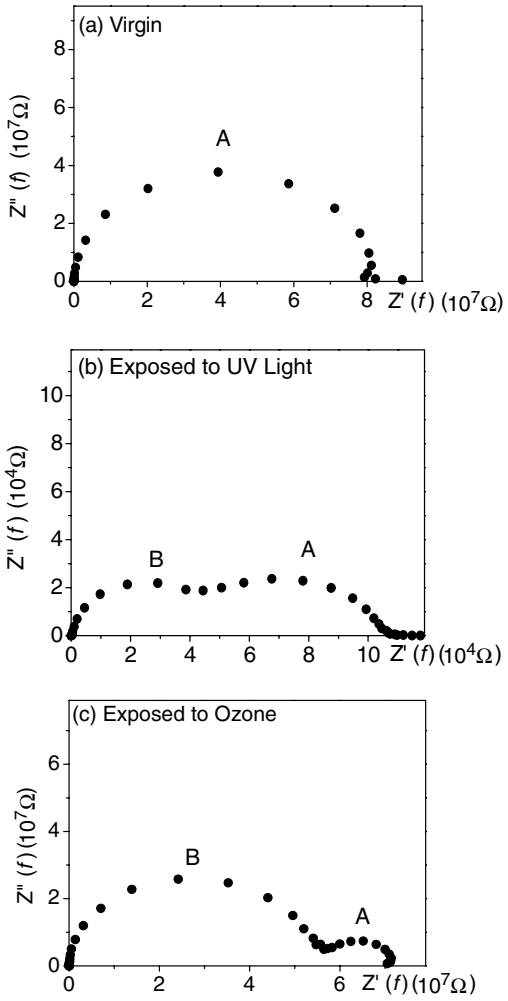

Fig. 2. Real, $z'(f)$, vs. imaginary, $z''(f)$, argand diagrams obtained from: (a) rf sputtering deposited ZnO film, (b) the same film after being irradiated by UV-light for 20 min, and (c) after to be exposed the sample to ozone atmosphere for 8 h.

effective impedance decreased from 90 MΩ to approximately 110 KΩ, while at 1 MHz it increased from 500 Ω to 2000 Ω. In addition, the dc effective impedance plateau was extended up to ~1 KHz, and a visible shoulder appeared just above 0.1 MHz, frequencies in which two maxima were recorded in the $z''(f)$ curve. Finally, Fig. 1(c) shows the measurement carried out with the same sample, now after the exposition to ozone atmosphere, which it is supposed to recover its original electric properties [11]. However, while at low frequency the impedance perfectly recovered its former value, at higher frequencies z' increased even more. It is also important to remark that the two peaks, in $z''(f)$ curve, also persist but they now shift to low frequencies.

The curves displayed in Fig. 2(a)–(c) are $z''(f) - z'(f)$ Argand diagrams of Fig. 1(a)–(c), respectively. Fig. 2(a) shows only one semicircle, here designated by A, indicating that only one transport mechanism takes place or, at least, dominates the transport process. It is represented by a unique relaxation time distribution. The response of the sample exposed to UV shows, on the other hand, two different mechanisms (Fig. 2(b)), that is, two relaxation time distributions are present, as shown by the two superimposed semicircles, A and B. This behaviour was expected since two peaks in the $z''(f)$ curve were recorded (Fig. 1(b)). $z''(f) - z'(f)$ of Fig. 2(c) shows that the semicircle B expanded over a major part of the frequency domain, while semicircle A shrunk even more due to the sample exposition to ozone atmosphere. These results clearly indicate that two transport mechanisms are under competition: that related to curve A (A-mechanism), which dominates in a virgin sample, and that of B (B-mechanism) that becomes prominent after UV and ozone exposition. Indeed the A-mechanism is dominant in the whole frequency domain in Fig. 2(a), but it loses progressively its field of action to B-mechanism as the ZnO-film is exposed either to UV or ozone gas.

4. Complex impedance model

Atomic force microscopy images and X-ray diffraction showed that S_{rf}-ZnO films, when deposited by rf magnetron sputtering, exhibit a crystalline-granular morphology, being the grains of about 90 nm in diameter [11]. In addition, EDX measurements proved that the stoichiometric Zn/O ratio does not change when a film is exposed either to UV or ozone gas. So, we may consider the film as composed by nanocrystalline regions separated by interfaces, as proposed by Martins et al. [11], and depicted in Fig. 3.

Therefore, the electronic conduction may be considered as a sum of two processes: one that takes into account barrier energies to be overcome by the carriers at the interfaces, and the other, another barrier energy distribution related to the internal grain structures. Based on these considerations we built a model for the conduction path in S_{rf}-ZnO films, in which carriers can migrate across the sample through the grains and/or the interstitial narrow regions between the grains. Therefore, two distinct regions were defined: one with complex permittivity ε_g^* related to the grains, and other with ε_i^* related to the interstitial regions. The whole film complex permittivity, $\varepsilon^*(\omega)$, is here described in terms of ε_g^* and ε_i^* by the bruggeman effective medium approximation (BEMA) [12]

$$f_g \frac{\varepsilon_g^* - \varepsilon^*}{\varepsilon_g^* + 2\varepsilon^*} + (1 - f_g) \frac{\varepsilon_i^* - \varepsilon^*}{\varepsilon_i^* + 2\varepsilon^*} = 0, \quad (1)$$

where f_g is the grains/film volume-fraction, and each complex permittivity is given by $\varepsilon^*(\omega) = -i\sigma^*(\omega)/\omega$. Further-

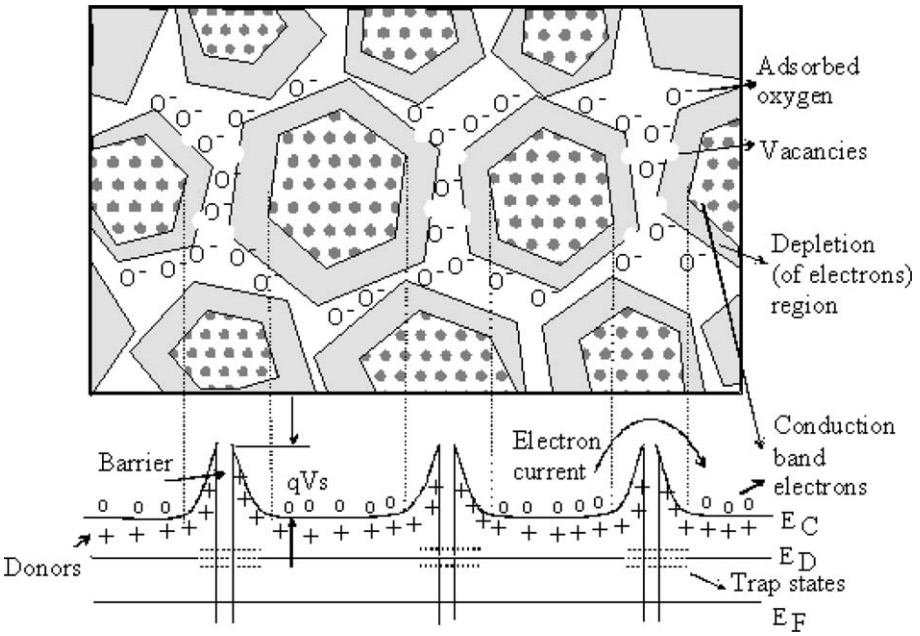

Fig. 3. Schematic model of the microstructure and corresponding energy bands of an oxide semiconductor obtained from Ref. [10].

Table 1
z_0^g and z_0^i parameters obtained from the fittings of the experimental curves of Fig. 1 and Eq. (3)

Sample	$z_0^g(\Omega)$	$z_0^i(\Omega)$
Virgin	1.0×10^8	6.3×10^8
Exposed to UV-light	9.1×10^4	8.3×10^6
Exposed to ozone	7.1×10^7	1.6×10^8

f_g was fixed at 0.85, and γ_{min}^g and γ_{min}^i are equal to the critical frequency displayed on Fig. 1.

more, the complex conductivities of the grain ($\sigma_g^*(\omega)$) and of the interface ($\sigma_i^*(\omega)$) are assumed to obey the random free energy barrier model (RFEB) [13,14], since the electronic conduction through these regions is via hopping mechanism among localized sites. For the RFEB model, the expression of the complex conductivity is given by [14]

$$\sigma_{g,i}^*(\omega) = \sigma_0^{g,i}\frac{i\omega/\gamma_{min}^{g,i}}{\ln(1+i\omega/\gamma_{min}^{g,i})}, \quad (2)$$

where $\sigma_0^{g,i}$ and $\gamma_{min}^{g,i}$ are respectively the dc effective impedance and the angular critical frequency related to the grain (σ_0^g, γ_{min}^g) and to the interstitial (σ_0^i, γ_{min}^i) regions.

From Eqs. (1) and (2) it is possible to obtain an expression for the complex impedance of the material, $z^*(\omega)$,

$$f_g\frac{z^*-z_g^*}{z^*+2z_g^*}+(1-f_g)\frac{z^*-z_i^*}{z^*+2z_i^*}=0, \quad (3)$$

where $z^*(\omega)=\ell/A\sigma^*(\omega)$ and $z_0^{g,i}=\ell/A\sigma_0^{g,i}$ is obtained from Eq. (2), being ℓ the film thickness and A the electrode area.

In Fig. 1 we exhibit the experimental-theoretical fittings for $z'(f)$ and $z''(f)$ obtained respectively from the virgin sample and after sample exposed to UV-light and to ozone gas. The adjusted parameters z_0^g and z_0^i are shown in Table 1. Despite the use of five parameters, only f_g can be considered as a real adjust parameter because the others (dc effective impedances and critical frequencies are taken from the experimental data). For these fitting f_g was fixed at 0.85. From Table 1 we observed that while both z_0^g and z_0^i decreased when the virgin sample was exposed to UV-light, they increased when the sample was exposed to ozone. Furthermore, z_0^g is always higher than z_0^i.

5. Conclusions

From the set of data obtained we notice that the S_{rf}-ZnO films exhibit two clear conduction mechanisms, as revealed by the $z'(f)$ vs $z''(f)$ plots. This behaviour can be modeled considering the S_{rf}-ZnO films as exhibiting a granular morphology to which it is applied the random free energy barrier (RFEB) model. By doing so, we saw that, for a virgin sample, the two mechanisms (A and B) are present and probably completely superimposed in the whole frequency range. The total impedance at low frequency (dc effective impedance) is around $10^8\ \Omega$, while for 1 MHz, the ac conductivity is around $10^3\ \Omega$. When the sample is exposed to UV-light, the mechanisms are spectroscopically separated, A shifts to low frequencies while B to high frequencies (see Fig. 2(b)). In this case, the dc effective conductivity of the films increases about three orders of magnitude, keeping unchanged that at high frequencies. On the other hand, if after UV-light exposure the sample is exposed to ozone gas, the B mechanism is expanded to lower frequencies; the dc effective conductivity recovers its former value while the high-frequency conductivities decreases. These data show that the UV acts in both the interstitial regions and grains, increasing its conductivities. From the point of view of the RFEB model this means that the average intensity of the energy barrier distributions decreases. On the other hand, when films are exposed to ozone gas, the films recovers its effective dc conductivity, which can be attributed to an increase of the height average of the barrier potential distributions.

Acknowledgements

This research was supported by the Fundação de Apoio ao Estado de São Paulo–Fapesp/Brazil and Millennium Science Initiative/MCT-Brazil and by the 'Fundação para a Ciência e a Tecnologia' through Pluriannual Contracts with CENIMAT and by the projects: POCTI/1999/ESE/35578, POCTI/1999/CTM/35440 and POCTI/2001/CTM/38924.

References

[1] A.R. Hutson, Phys. Rev. Lett. 4 (1960) 505.
[2] M. Matsuoka, Advances in Ceramics, vol. 1, American Ceramic Society, Westerville, OH, 1981.
[3] P. Durán, F. Capel, J. Tartaj, C. Moure, Adv. Mater. 14 (2002) 137.
[4] A.K. Ghosh, T.K. Munshi, Indian J. PHYS. and Procced. The Iindian Assoc. for the Cult. Sci. Part A 77A (6) (2003) 637.
[5] C.R. Wuethrich, C.A.P. Muller, G.R. Fox, H.G. Limberger, Sensor Actuat. A-Phys. 66 (1998) 114.
[6] G.D. Mahan, L.M. Levinson, H.R. Philips, J. Appl. Phys. 50 (1979) 2799.
[7] M. Bender, E. Fortuato, P. Nunes, I. Ferreira, A. Marques, R. Martins, N. Katsarakis, V. Cimalla, G. Kiriakidis, Jpn. J. Appl. Phys. 42 (2003) L435.
[8] X. Jiang, F.L. Wong, M.K. Fung, S.T. Lee, Appl. Phys. Lett. 83 (2003) 1875.
[9] E.M.C. Fortunato, P.M.C. Barquinha, A.C.M.B.G. Pimentel, A.M.F. Gonçalves, A.J.S. Marques, R.F.P. Martins, App. Phys. Lett. 85 (2004) 2541.
[10] Z.L. Wang, Mater. Today 7 (2004) 26.
[11] R. Martins, E. Fortunato, P. Nunes, I. Ferreira, A. Marques, M. Bender, N. Katsarakis, V. Cimalia, G. Kiriakidis, J. Appl. Phys. 96 (2004) 1398.
[12] D.E. Aspnes, Thin Solid 89 (1982) 249.
[13] J.C. Dyre, J. Appl. Phys. 64 (1988) 2456.
[14] R.F. Bianchi, G.F. Leal Ferreira, C.M. Lepienski, R.M. Faria, J. Chem. Phys. 110 (1999) 4602.